Proc. Indian Acad. Sci. (Math. Sci.), Vol. 91, Number 1, January 1982, pp. 17–37.

Oberbeck convection through vertical porous stratum

N RUDRAIAH, M VENKATACHALAPPA and
M S MALASHETTY
UGC-DSA Centre in Fluid Mechanics, Department of Mathematics, Central College, Bangalore University, Bangalore 560 001, India

MS received 30 November 1981

Abstract. Natural convection through a vertical porous stratum is investigated both analytically and numerically. Analytical solutions are obtained using a perturbation method valid for small values of buoyancy parameter N and the numerical solutions are obtained using Runge-Kutta-Gill method. It is shown that analytical solutions are valid for $N < 1$ and several features of the effect of large values of N are reported. The combined effects of increase in the values of temperature difference between the plates and the permeability parameter on velocity, temperature, mass flow rate and the rate of heat transfer are reported. It is shown that higher temperature difference is required to achieve the mass flow rate in a porous medium equivalent to that of viscous flow.

Keywords. Oberbeck convection; vertical porous stratum; Runge-Kutta-Gill method; buoyancy parameter.

1. Introduction

Density differences in fluid saturated vertical porous medium, interacting with the gravitational field, produces an immense diversity of buoyancy forces and flow configurations in nature and in process of technology; particularly in petroleum and chemical industries. It is also of interest in geohydrology where the flow pattern in heated ground water possesses features of a vertical convection column into which cold ground water is being entrained (see Wooding [7]).

The study of motion of ground water is usually based on the Darcy law [2] in which the macroscopic length scale of a system is so large that the diffusion effects are neglected. However, in zones of mixing between fluids at different temperatures the diffusion effects are significant since the gradients of fluid properties are large. In these zones, the nature of fluid motion is such that boundary layer approximations are valid and the usual potential nature of Darcy equation is not valid. An exact mathematical model to account for the boundary layer aspect in a porous medium is not yet available to our knowledge. To a first approximation, however, we can use the Brinkman model (Rudraiah and Nagaraj [5]). Flows obeying Brinkman model might be found in geothermal areas or might arise from the heat generated by deep explosions in saturated ground.

Therefore, recently Rudraiah and Nagaraj [5] have investigated natural convection in a vertical porous stratum using the Brinkman [1] model and maintaining the boundaries at the same temperature. However, in many practical problems cited above one usually encounters the Oberbeck type of convection (maintaining the temperature gradient in a direction normal to gravity) for which the boundaries have to be maintained at different temperatures; viz., one is maintained at a higher temperature than the other. This Oberbeck problem, in the usual viscous case (that is absence of a porous medium), has been extensively studied (see Gebhart [3]) but much attention has not been given in the case of a porous medium. Recently, Rudraiah and Nagaraj [5] have obtained analytical solutions in a vertical porous layer using a regular perturbation technique which are true only for small values of buoyancy parameter N. It is of interest to know up to what values of N the analytical solutions are valid. These aspects are investigated in this paper using the following plan of work.

The Brinkman equations and the corresponding boundary conditions are given in §2. Analytical solutions for small values of the buoyancy parameter N are obtained in §3. To know up to what values of N the analytical solutions are valid, the basic equations are numerically integrated in §4, using Runge-Kutta-Gill method for wide range of values of N. The effect of permeability and buoyancy parameter N on the skin friction and rate of heat transfer are also calculated. The results are discussed in §5. It is shown that the analytical solutions are valid for values of $N < 1$.

2. Basic equations

The physical model, shown in figure 1, consists of vertical porous stratum bounded by two rigid plates at $y = \pm b$ with x-axis in the axial direction and y-axis perpendicular to the plates. We assume that steady Boussinesq fluid percolating through a homogeneous isotropic porous medium in the x-direction and physical quantities vary with respect to y. Buoyancy forces, due to density difference,

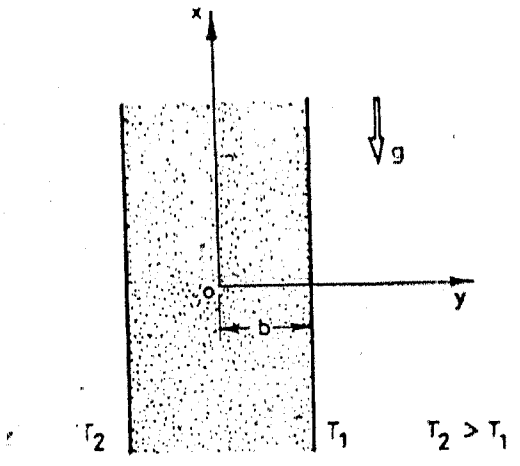

Figure 1. Physical configuration of flow.

cause the fluid to flow upwards through the channel. For this flow, the basic equations of motion, following Rudraiah and Nagaraj [5], are

$$\frac{d^2 u}{dy^2} - \frac{u}{k} + \frac{g\beta (T - T_0)}{\nu} = 0, \tag{1}$$

$$\frac{d^2 T}{dy^2} + \frac{\rho_0 \nu}{K}\left(\frac{du}{dy}\right)^2 + \frac{\rho_0 \nu}{kK} u^2 = 0, \tag{2}$$

$$\rho = \rho_0 [1 - \beta (T - T_0)], \tag{3}$$

where u is the velocity component in the x-direction, T the temperature, T_0 the ambient temperature at $\rho = \rho_0$, ρ the density of the fluid, ν the kinematic viscosity, K the thermal conductivity, k the permeability of a porous medium and β the coefficient of thermal expansion. These equations are solved using the boundary conditions

$$u = 0 \text{ at } y = \pm b, \tag{4}$$

$$T = T_1 \text{ at } y = + b, \tag{5}$$

$$T = T_2 \text{ at } y = - b. \tag{6}$$

The boundary condition on velocity represents the noslip condition and that on temperature points to the fact that the plates are isothermally maintained at different temperatures T_1 and T_2 ($T_2 > T_1$). Equations (1) and (2), using the dimensionless quantities

$$y^* = \frac{y}{b}, \quad \theta = \frac{T - T_0}{T_1 - T_0}, \quad u^* = \frac{\nu}{g\beta b^2 (T_1 - T_0)} u, \tag{7}$$

and for simplicity neglecting the asterisk (*), become

$$\frac{d^2 u}{dy^2} - \sigma^2 u + \theta = 0, \tag{8}$$

$$\frac{d^2 \theta}{dy^2} + N\left(\frac{du}{dy}\right)^2 + N\sigma^2 u^2 = 0, \tag{9}$$

where

$\sigma = b/\sqrt{k}$ is the permeability parameter and

$N = \dfrac{\rho_0 g^2 b^4 \beta^2 (T_1 - T_0)}{\nu K}$ is the buoyancy parameter.

Since the flow is caused by the buoyancy force, the velocity is made dimensionless using this force. The corresponding boundary conditions are

$$u = 0 \quad \text{at} \quad y = \pm 1, \tag{10}$$

$$\theta = 1 \quad \text{at} \quad y = 1, \tag{11}$$

$$\theta = 1 + \bar{\theta} \quad \text{at} \quad y = -1, \tag{12}$$

where

$$\bar{\theta} = \frac{T_2 - T_1}{T_1 - T_0}. \tag{13}$$

At first sight it appears reasonable to ignore the dissipative effects in (9). However, the propagation of waves in a porous medium has small free decay time and hence considerable dissipative effects. Thus the accurate description of flow in a porous medium must include dissipative effects. Therefore (8) and (9) are coupled non-linear equations because of the dissipation term which must be solved simultaneously to yield the desired velocity and temperature profiles. Due to the non-linearity, analytical solutions of these equations are difficult. However if N is small such solutions, following Rudraiah and Nagaraj [5], can be obtained using a regular perturbation technique. This is done in §3, with the motive of understanding the dissipative effects on the flow. To know the validity of these solutions and to find the effects of large N on the flow, (8) and (9) are solved numerically in §4.

3. Analytical solutions

When the buoyancy parameter N is very small we look for solutions of (8) and (9) in the form

$$u = u_0 + Nu_1 + N^2 u_2 + \ldots, \tag{14}$$

$$\theta = \theta_0 + N\theta_1 + N^2 \theta_2 + \ldots, \tag{15}$$

where zero subscript quantities are the solutions for the case $N = 0$, which represents physically the solutions in the absence of viscous and Darcy dissipations and $u_1, u_2 \ldots, \theta_1, \theta_2 \ldots$ represents the perturbation quantities relating to u_0 and θ_0. Substituting (14) and (15) into (8)-(12) and equating the coefficients of the like powers of N to zero we get the following set of equations.

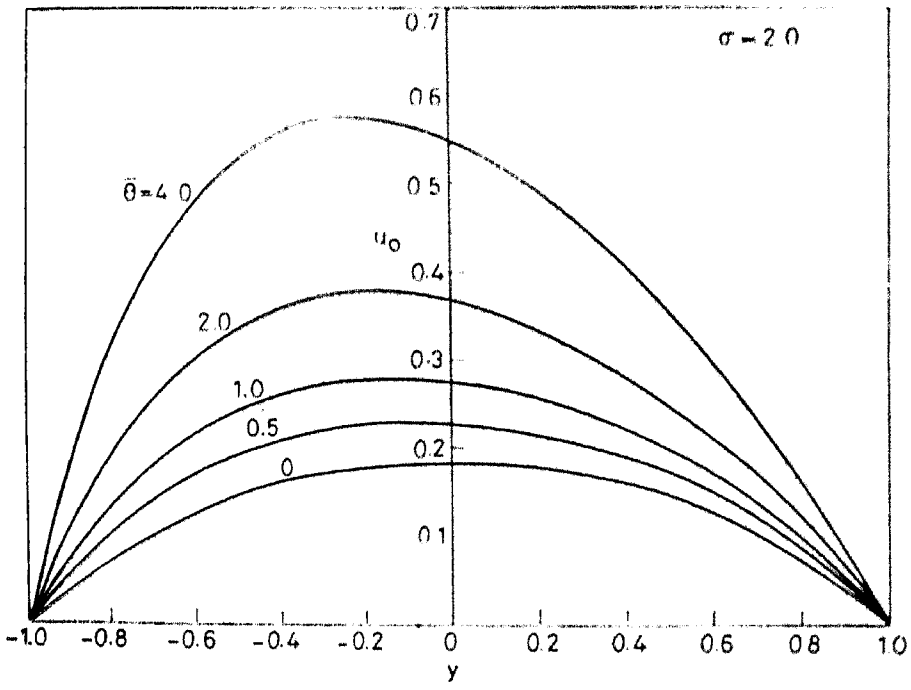

Figure 2. Velocity profiles for various $\bar{\theta}$ (when dissipations are neglected).

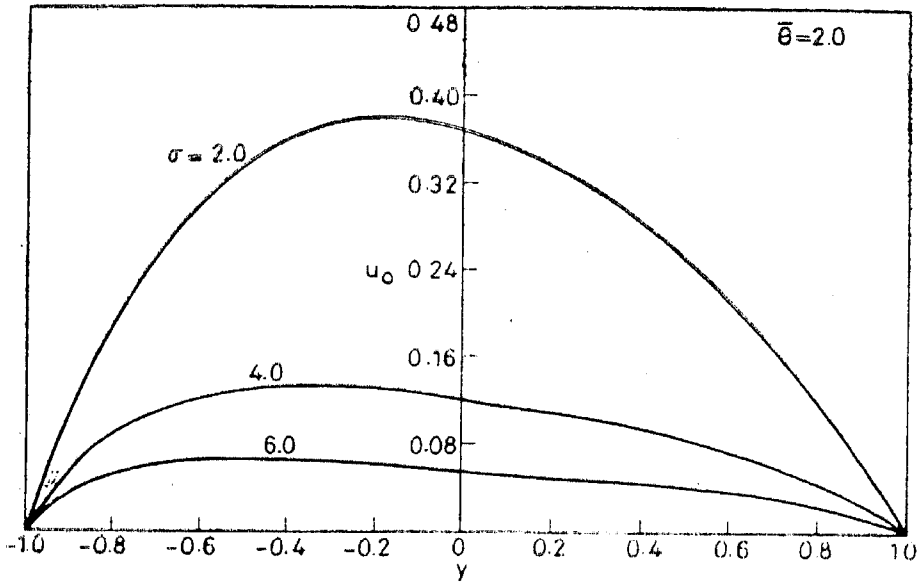

Figure 3. Velocity profiles for various σ (when dissipations are neglected).

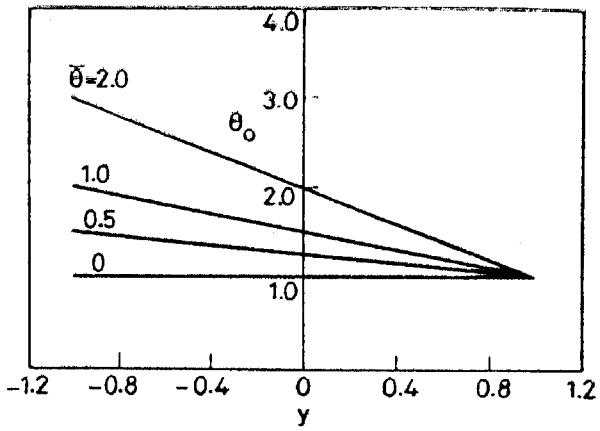

Figure 4. Temperature profiles (when dissipations are neglected).

Zeroth order equations

$$\frac{d^2 u_0}{dy^2} - \sigma^2 u_0 + \theta_0 = 0, \tag{16}$$

$$\frac{d^2 \theta_0}{dy^2} = 0. \tag{17}$$

First order equations

$$\frac{d^2 u_1}{dy^2} - \sigma^2 u_1 + \theta_1 = 0, \tag{18}$$

$$\frac{d^2 \theta_1}{dy^2} + \left(\frac{du_0}{dy}\right)^2 + \sigma^2 u_0^2 = 0, \tag{19}$$

The corresponding boundary conditions are

$$u_0 = 0 \quad \text{at} \quad y = \pm 1, \tag{20}$$

$$\theta_0 = 1 \quad \text{at} \quad y = +1, \tag{21}$$

$$\theta_0 = 1 + \bar{\theta} \quad \text{at} \quad y = -1, \tag{22}$$

and $$u_i = \theta_i = 0 \text{ at } y = \pm 1,\ i = 1, 2, \ldots. \tag{23}$$

The solutions of (16) and (17) using the boundary conditions (20)–(22) are

$$u_0 = \frac{1}{\sigma^2}\left[1 - \frac{\cosh\sigma y}{\cosh\sigma}\right] + \frac{\bar{\theta}}{2\sigma^2}\left[\frac{\sinh\sigma y}{\sinh\sigma} - \frac{\cosh\sigma y}{\cosh\sigma} - y + 1\right], \tag{24}$$

$$\theta_0 = 1 + \frac{\bar{\theta}}{2}\,[1 - y]. \tag{25}$$

In the limit $\sigma \to 0$, (24) tends to

$$u_{0_0} = \frac{1}{2}\,[1 - y^2] + \frac{\bar{\theta}}{12}\,[y^3 - 3y^2 - y + 3]. \tag{26}$$

which is the velocity distribution in the channel in the absence of porous material, called viscous flow solutions. When $\bar{\theta} = 0$ that is when the plates are maintained at the same temperature (24) and (25) reduce to those given by Rudraiah and Nagaraj [5]. The second term on the right hand side of (24) and (25) are the contributions from maintaining the plates at different temperatures. Equations (24) and (25) are computed for different values of $\bar{\theta}$ and σ which are shown in figures 2-4 and the results are discussed in § 5.

The solutions of (18) and (19), using the boundary conditions (23), are

$$\begin{aligned} u_1 = {} & f_1(\sigma)\frac{\cosh\sigma y}{\cosh\sigma} - \left[\frac{y}{\sigma^5}\cdot\frac{\sinh\sigma y}{\cosh\sigma} - \frac{\cosh 2\sigma y}{12\sigma^6\cosh^2\sigma} + \frac{y^2}{2\sigma^4}\right] \\ & - f_2(\sigma) + \bar{\theta}^2\left[f_3(\sigma)\frac{\cosh\sigma y}{\cosh\sigma} - f_4(\sigma)\frac{\sinh\sigma y}{\sinh\sigma}\right] \\ & + \frac{\bar{\theta}^2}{4\sigma^4}\left\{\frac{\coth 2\sigma}{3\sigma^2}\cdot\frac{\cosh 2\sigma y}{\sinh 2\sigma} + \frac{y(1-y^2)}{\sigma}\left[\frac{\cosh\sigma y}{\sinh\sigma} - \frac{\sinh\sigma y}{\cosh\sigma}\right]\right. \\ & + \frac{3y^2}{2\sigma^2}\left[\frac{\sinh\sigma y}{\sinh\sigma} - \frac{\cosh\sigma y}{\cosh\sigma}\right] - \frac{\sinh 2\sigma y}{3\sigma^2\sinh 2\sigma} - \frac{y^4}{12} + \frac{y^3}{3} \\ & \left. + \frac{(\sigma^2+2)}{2\sigma^2}y^2 + \frac{2y}{\sigma^2} - \frac{1}{\sigma^2} - \frac{2}{\sigma^4}\right\} + \bar{\theta}\left[f_5(\sigma)\frac{\cosh\sigma y}{\cosh\sigma}\right. \\ & \left. - 2f_4(\sigma)\frac{\sinh\sigma y}{\sinh\sigma}\right] + \frac{\bar{\theta}}{\sigma^4}\left\{\frac{\cosh 2\sigma y}{12\sigma^2\cosh^2\sigma} - \frac{y\sinh\sigma y}{\sigma\cosh\sigma}\right. \\ & + \frac{y^2}{4\sigma}\cdot\frac{\sinh\sigma y}{\cosh\sigma} + \frac{y}{2\sigma}\cdot\frac{\cosh\sigma y}{\sinh\sigma} - \frac{1}{6\sigma^2}\frac{\sinh 2\sigma y}{\sinh 2\sigma} - \frac{3y\cosh\sigma y}{4\sigma^2\cosh\sigma} \\ & \left. + \frac{y^3}{6} - \frac{y^2}{2} + \frac{(y-1)}{\sigma^2}\right\} + f_6(\sigma)\left[1 - \frac{\cosh\sigma y}{\cosh\sigma}\right] \\ & + f_7(\sigma)\left[\frac{\sinh\sigma y}{\sinh\sigma} - y\right], \end{aligned} \tag{27}$$

$$\theta_1 = \frac{2}{\sigma^4}\cdot\frac{\cosh\sigma y}{\cosh\sigma} - \frac{1}{4\sigma^4}\frac{\cosh 2\sigma y}{\cosh^2\sigma} - \frac{y^2}{2\sigma^2} + f_8(\sigma)$$
$$- \frac{\bar\theta^2}{4\sigma^2}\left[\frac{\cosh 2\sigma}{\sigma^2\sinh^2 2\sigma}\cdot\cosh 2\sigma y - \frac{\sinh 2\sigma y}{\sigma^2\sinh 2\sigma} + \frac{2}{\sigma^2}(1-y)\frac{\sinh\sigma y}{\sinh\sigma}\right.$$
$$- \frac{2}{\sigma^2}(1-y)\frac{\cosh\sigma y}{\cosh\sigma} + \frac{2}{\sigma^3}\left(\frac{\cosh\sigma y}{\sinh\sigma} - \frac{\sinh\sigma y}{\cosh\sigma}\right) + \frac{y^4}{12}$$
$$\left. - \frac{y^3}{3} + \frac{y^2}{2}\right] + \frac{\bar\theta}{\sigma^2}\left[\frac{1}{\sigma^2}\left(\frac{\sinh\sigma y}{\sinh\sigma} - 2\frac{\cosh\sigma y}{\cosh\sigma}\right)\right.$$
$$- \frac{\sinh 2\sigma y}{2\sigma^2\sinh 2\sigma} + \frac{\cosh 2\sigma y}{4\sigma^2\cosh^2\sigma} + \frac{y\cosh\sigma y}{\sigma^2\cosh\sigma} - \frac{1}{\sigma^3}\frac{\sinh\sigma y}{\cosh\sigma}$$
$$\left. - \frac{y^3}{6} + \frac{y^2}{2}\right] + f_6(\sigma)\cdot y + f_7(\sigma), \tag{28}$$

where

$$f_1(\sigma) = \frac{3}{\sigma^6} + \frac{\tanh\sigma}{\sigma^5} - \frac{\cosh 2\sigma}{3\sigma^6\cosh^2\sigma},$$

$$f_2(\sigma) = \frac{3}{\sigma^6} - \frac{\cosh 2\sigma}{4\sigma^6\cosh^2\sigma} - \frac{1}{2\sigma^4},$$

$$f_3(\sigma) = \frac{1}{4\sigma^4}\left[-\frac{\coth^2 2\sigma}{3\sigma^2} + \frac{\coth\sigma}{2\sigma} + \frac{\tanh\sigma}{\sigma} + \frac{2}{\sigma^4} + \frac{1}{2\sigma^2} + \frac{7}{12}\right],$$

$$f_4(\sigma) = \frac{1}{4\sigma^4}\left[\frac{\coth\sigma}{\sigma} + \frac{\tanh\sigma}{2\sigma} + \frac{1}{6\sigma^2} + \frac{1}{3}\right],$$

$$f_5(\sigma) = \frac{1}{\sigma^4}\left[-\frac{\cosh 2\sigma}{12\sigma^2\cosh^2\sigma} + \frac{\tanh\sigma}{\sigma} + \frac{1}{\sigma^2} + \frac{1}{2}\right],$$

$$f_6(\sigma) = \frac{\bar\theta^2}{4\sigma^2}\left[\frac{\cosh^2 2\sigma}{\sigma^2\sinh^2 2\sigma} + 2\frac{\coth\sigma}{\sigma^3} - \frac{4}{\sigma^2} + \frac{7}{12}\right]$$
$$+ \frac{\bar\theta}{\sigma^2}\left[\frac{\cosh 2\sigma}{4\sigma^2\cosh^2\sigma} - \frac{2}{\sigma^2} + \frac{1}{2}\right],$$

$$f_7(\sigma) = \frac{\bar\theta(\bar\theta+2)}{2\sigma^2}\left[\frac{\tanh\sigma}{\sigma^3} - \frac{3}{2\sigma^2} + \frac{1}{6}\right],$$

and

$$f_8(\sigma) = \frac{1}{4\sigma^4}\cdot\frac{\cosh 2\sigma}{\cosh^2\sigma} - \frac{2}{\sigma^4} + \frac{1}{2\sigma^2}.$$

Equations (27) and (28) are evaluated for different values of σ and $\bar\theta$ and the results are shown in figures 5 and 6.

It is of practical interest to find the mass flow rate and friction factor. The mass flow rate depicts quantitatively the effect of permeability on the flow and the friction factor gives information as to under what Reynolds number the flow is laminar.

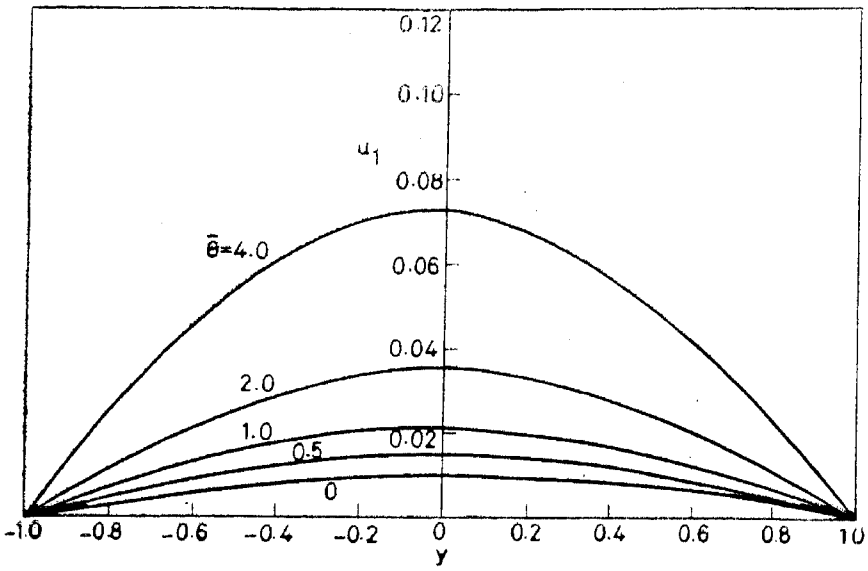

Figure 5. Velocity correction profiles for different $\bar{\theta}$ and $\sigma = 2{\cdot}0$.

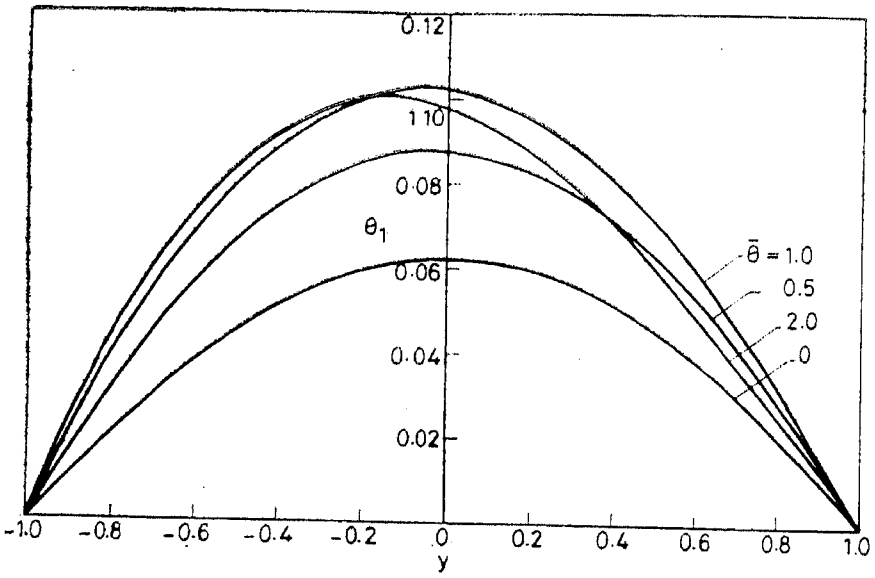

Figure 6. Temperature correction profiles for different $\bar{\theta}$ and $\sigma = 2{\cdot}0$.

If M_{x_0} denotes the mass flow rate per unit channel width in the absence of dissipation (i.e., $N = 0$) then

$$M_{x_0} = \int_{-b}^{+b} \rho_0 u_0 dy,$$

$$= -\frac{\rho_0 G b^3}{\sigma^2}(2 + \bar{\theta})\left[1 - \frac{\tanh \sigma}{\sigma}\right], \tag{29}$$

where

$$G = -\frac{g\beta(T_1 - T_0)}{\nu}.$$

On the other hand if M_{f0} denotes the mass flow rate per unit channel width for viscous flow then

$$M_{f_0} = -\frac{\rho_0 G b^2}{3}(2 + \bar{\theta}). \tag{30}$$

For the conditions of equal pressure gradients and channel width the ratio of equation (29) to (30) gives

$$\frac{M_{\rho_0}}{M_{f_0}} = \frac{3}{\sigma^2}\left[1 - \frac{\tanh\sigma}{\sigma}\right] \tag{31}$$

which is independent of $\bar{\theta}$ because of the neglection of dissipative effects. This ratio of mass flow rates is computed for different values of σ and is shown in figure 7. From this it is clear that mass flow rate decreases with increase in σ.

Now the friction factor C_f is defined by

$$C_f = -\frac{\nu G D}{\frac{1}{2}\bar{u}_0^2}, \tag{32}$$

where D is the equivalent diameter ($D = 4b$ for the channel considered in this paper).

Since

$$\bar{u}_0 = \frac{1}{2\bar{b}}\int_{-b}^{+b} u_0\, dy,$$

$$= -\frac{Gb^2}{2\sigma^2}(2 + \bar{\theta})\left[1 - \frac{\tanh\sigma}{\sigma}\right], \tag{33}$$

we get

$$C_f = \frac{64\sigma^2}{\mathrm{Re}\,(2 + \bar{\theta})\left[1 - \frac{\tanh\sigma}{\sigma}\right]}, \tag{34}$$

where

$\mathrm{Re} = \frac{u_0 D}{\nu}$ is the Reynolds number.

Thus

$$C_f\,\mathrm{Re} = \frac{64\sigma^2}{(2 + \bar{\theta})\left[1 - \frac{\tanh\sigma}{\sigma}\right]}. \tag{35}$$

This shows that the product C_fRe is constant (independent of a Reynolds number) for a channel of fixed width and a given porous medium. This product, in the case of usual viscous flow through a channel, is

$$C_f^*\,\mathrm{Re}^* = \frac{192}{(2 + \bar{\theta})}. \tag{36}$$

The ratio of (35) to (36) is

$$\frac{C_f\,\mathrm{Re}}{C_f^*\,\mathrm{Re}^*} = \frac{\sigma^2}{3\,[1 - \tanh\sigma/\sigma]}, \tag{37}$$

which depends only on the permeability of a porous medium and the width of the channel. This ratio is numerically evaluated for different values of σ and is shown in figure 8. From this it is clear that the ratio increases with increase in σ. Thus for large value of σ the flow is laminar.

Once the velocity distribution is known, the skin friction can be calculated from

$$\tau' = \mu \left(\frac{\partial u}{\partial y}\right)_{y=\pm b}, \tag{38}$$

which in the non-dimensional form can be written, by using (7), as

$$\begin{aligned} \tau &= \frac{\tau'}{\rho g b (T_1 - T_0)}, \\ &= \left(\frac{du}{dy}\right)_{y=\pm 1}, \\ &= \left(\frac{du_0}{dy} + N\frac{du_1}{dy}\right)_{y=\pm 1}. \end{aligned} \tag{39}$$

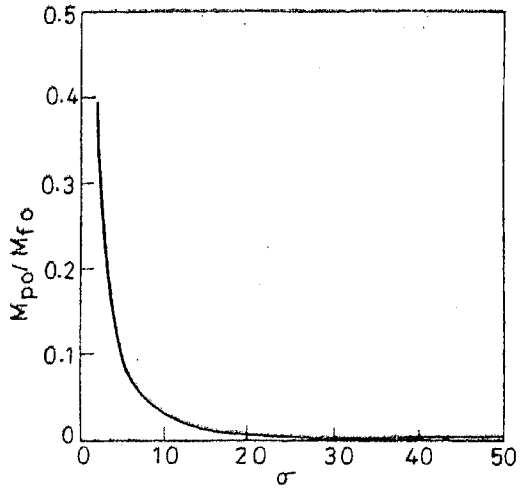

Figure 7. Ratio of mass flow rate with and without porous medium *versus* σ.

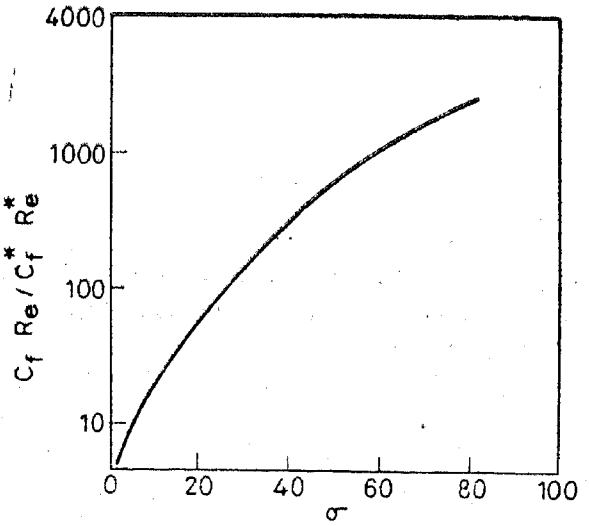

Figure 8. Ratio of the product of friction factor and Reynolds number with and without porous medium *versus* σ.

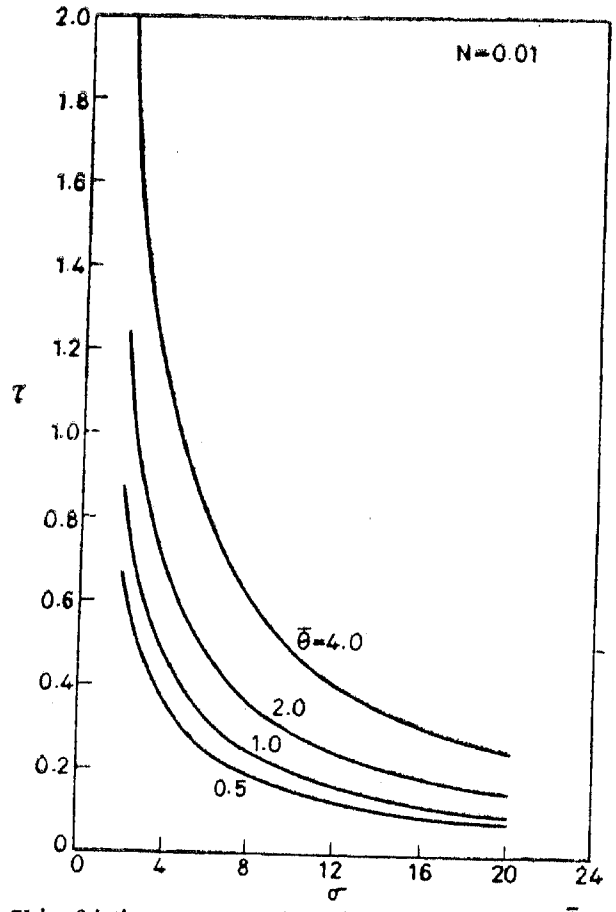

Figure 9. Skin friction *versus* σ for different values of $\bar{\theta}$ at hotter plate.

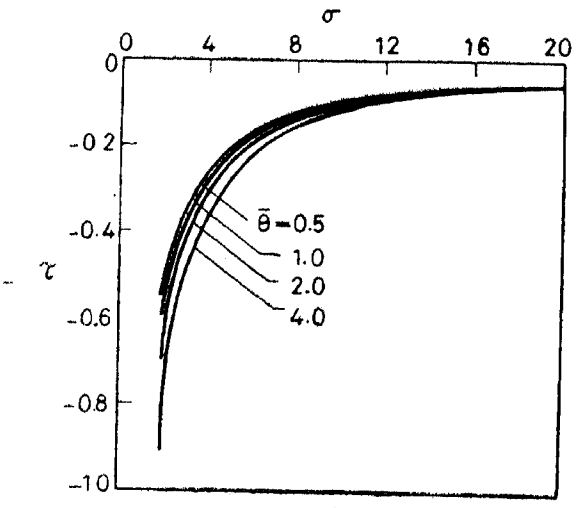

Figure 10. Skin friction *versus* σ for different values of $\bar{\theta}$ at cooler plate.

τ is plotted against σ in figures 9 and 10, for $N = 0{\cdot}01$ and for different values of $\bar{\theta}$.

It is of practical interest and importance to calculate the rate of heat transfer between the fluid and the plates. This is given by

$$q' = -K\left(\frac{\partial T}{\partial y}\right)_{y=\pm b}, \tag{40}$$

which in the non-dimensional form can be written using (7) as

$$q = \frac{-q'\,b}{K(T_1 - T_0)},$$

$$= \left(\frac{d\theta}{dy}\right)_{y=\pm 1}, \tag{41}$$

$$= \left(\frac{d\theta_0}{dy} + N\frac{d\theta_1}{dy}\right)_{y=\pm 1}. \tag{42}$$

q is plotted against σ in figures 11 and 12 for $N = 0{\cdot}01$ and for different values of $\bar{\theta}$.

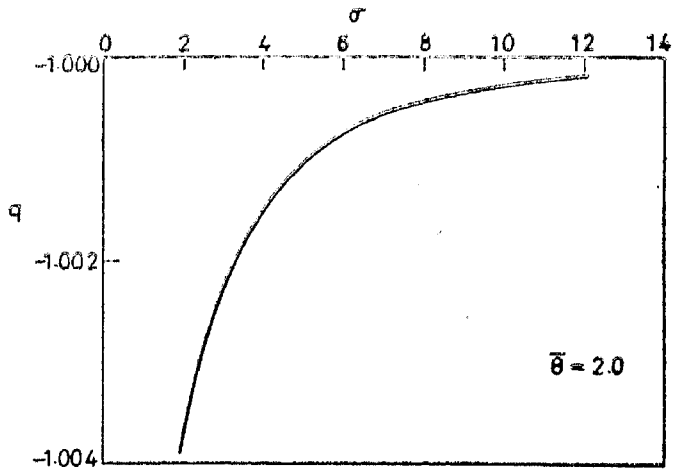

Figure 11. Rate of heat transfer for various σ at hotter plate.

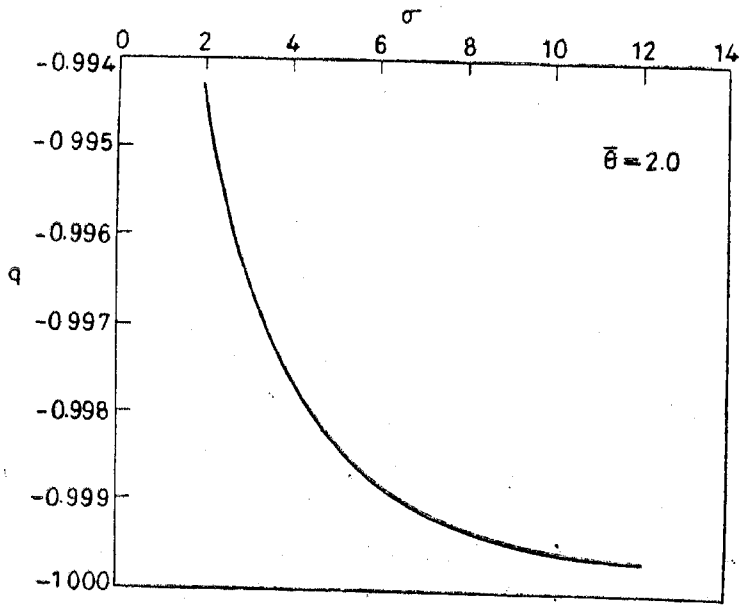

Figure 12. Rate of heat transfer for various σ at cooler plate.

4. Numerical solutions

The analytical solutions obtained in §3 are valid only for small values of the buoyancy parameter N. To know the validity of the analytical solutions and to find the effect of large N on the flow we have solved (8) and (9) with the boundary conditions (10)–(12) numerically, using Runge–Kutta–Gill method.

The numerical method involves solving a non-linear two point boundary value problem using an iterative scheme. We have used a slightly modified method and the FORTRAN program developed by Sen and Venkataramudu [6]. The velocity and temperature distributions are obtained for a wide range of values of N and are shown in figures 13 and 14. We find that the analytical solutions are in very good agreement with the numerical solutions when N is very small. For the sake of comparison we have given the values of velocity and temperature at $y = 0$ for $\bar{\theta} = 1{\cdot}0$ and $\sigma = 2{\cdot}0$ in tables 1 and 2.

The mass flow rate and friction factor found in §3 are true only in the absence of dissipations. Here we find the mass flow rate and friction factor in the presence of dissipative effects.

Let M_p denote the mass flow rate per unit channel width in the presence of dissipations, then

$$M_p = \int_{-b}^{+b} \rho_0 u dy,$$

$$= -\rho_0 G b^3 \int_{-1}^{+1} u dy. \tag{43}$$

Let M_f denote the mass flow rate per unit channel width in the presence of dissipation for viscous flow, then

$$M_f = -\rho_0 G b^3 \int_{-1}^{+1} u_f dy. \tag{44}$$

The ratio of (43) to (44) is

$$\frac{M_p}{M_f} = \frac{\int_{-1}^{+1} u dy}{\int_{-1}^{+1} u_f \, dy}. \tag{45}$$

The friction factor C_f is defined as

$$C_f = -\frac{\nu G D}{\frac{1}{2}\bar{u}^2}, \tag{46}$$

where

$$\bar{u} = \frac{1}{2b} \int_{-b}^{+b} u dy,$$

$$= -\frac{G b^2}{2} \int_{-1}^{+1} u dy. \tag{47}$$

Equation (46) using (47) becomes

$$C_f = \frac{64}{\mathrm{Re} \int_{-1}^{+1} u dy}, \tag{48}$$

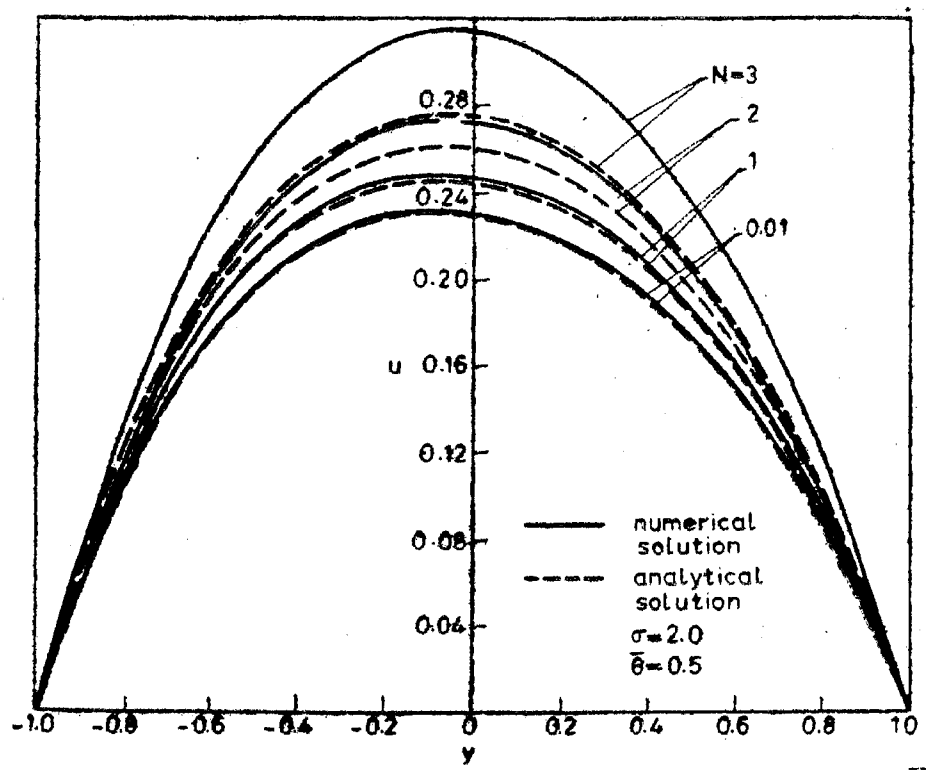

Figure 13. Velocity profiles.

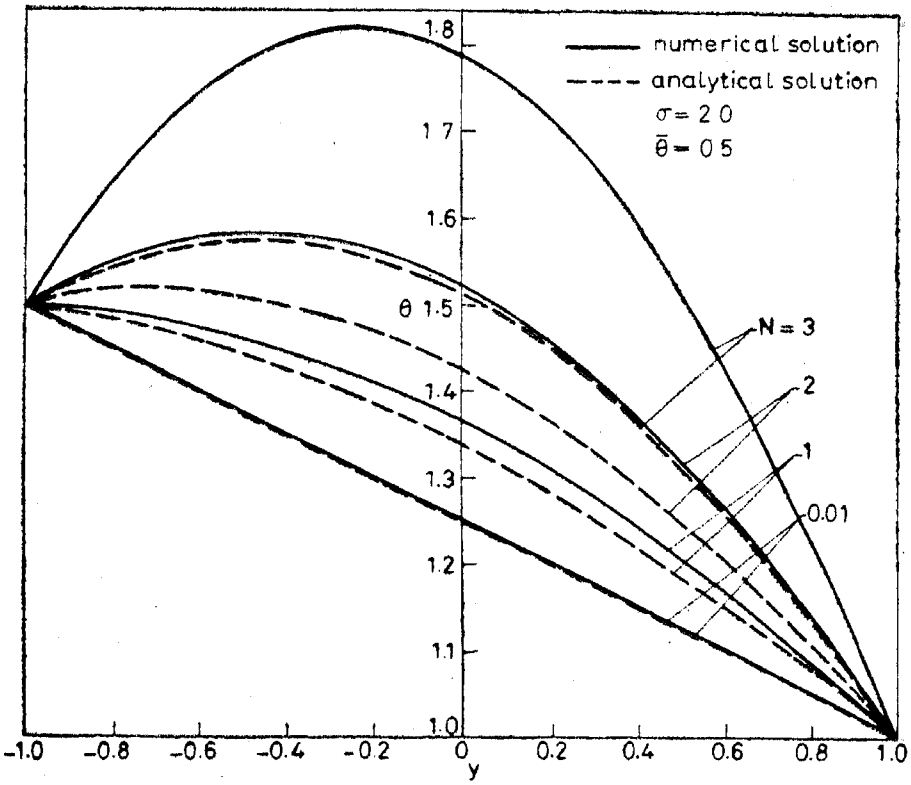

Figure 14. Temperature profiles.

Table 1. Velocity at $y = 0$, $\bar{\theta} = 1{\cdot}0$, $\sigma = 2{\cdot}0$.

N	Numerical	Analytical
0·01	0·2758473	0·2755308
0·05	0·2764471	0·2763725
0·1	0·2778879	0·2774250
0·2	0·2799254	0·279530
0·3	0·2823414	0·2816350
0·4	0·2848408	0·283740
0·5	0·2874295	0·288845
0·6	0·2901138	0·289580
0·7	0·2928998	0·290055
0·8	0·2957960	0·292160
0·9	0·2988109	0·294265

Table 2. Temperature at $y = 0$, $\bar{\theta} = 1{\cdot}0$, $\sigma = 2{\cdot}0$.

N	Numerical	Analytical
0·01	1·501418	1·501025
0·05	1·507135	1·5051260
0·1	1·514384	1·510252
0·2	1·529239	1·520504
0·3	1·544593	1·530756
0·4	1·560480	1·541008
0·5	1·576935	1·551260
0·6	1·593999	1·561512
0·7	1·611715	1·571764
0·8	1·630132	1·582016
0·9	1·649305	1·592268

where

$\mathrm{Re} = \dfrac{\bar{u}D}{\nu}$ is the Reynolds number.

Thus

$$C_f \mathrm{Re} = \frac{64}{\int_{-1}^{+1} u\,dy}. \tag{49}$$

This product in the case of viscous flow is

$$C_f^* \mathrm{Re}^* = \frac{64}{\int_{-1}^{+1} u_f\,dy} \tag{50}$$

The ratio of (49) to (50) is

$$\frac{C_f \, \mathrm{Re}}{C_f^* \, R_\sigma^*} = \frac{\int_{-1}^{+1} u_f \, dy}{\int_{-1}^{+1} u \, dy}. \tag{51}$$

Equations (45) and (51) are evaluated numerically for different values of N and are shown in figures 15 to 17.

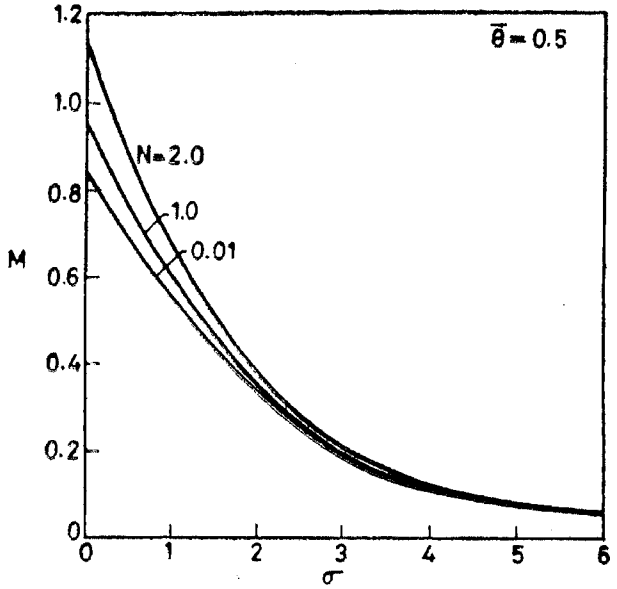

Figure 15. Mass flow rate *vs.* σ for different N.

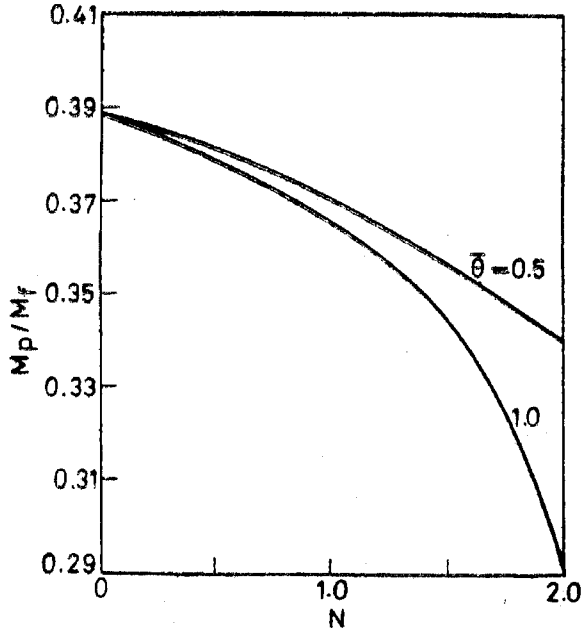

Figure 16. Ratio of mass flow rate *vs.* N for $\sigma = 2{\cdot}0$.

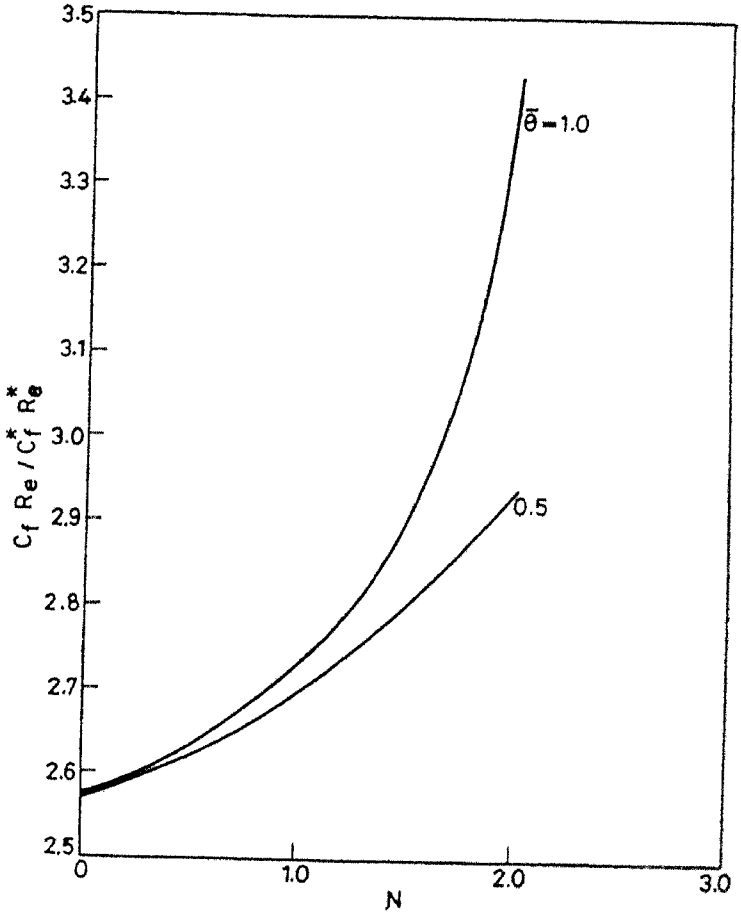

Figure 17. Ratio of the product of friction factor and Reynolds number *vs. N*.

The skin friction and the rate of heat transfer defined by (38) and (40) are numerically evaluated for different values of N and σ and are shown in figures 18 to 21.

5. Discussion

The direct analytical solutions for the problem of natural convection through a vertical porous stratum can be obtained in the absence of dissipative effects. In the presence of dissipative effects, however, analytical solutions are obtained by a regular perturbation method valid for small values of N and the results are shown in figures 2 to 12. Figures 2 to 4 are concerned with velocity and temperature distributions in the absence of dissipative effects. The effect of increase in the temperature difference between the plates, viz., $\bar{\theta}$, is to increase the velocity and temperature distributions (see figures 2 and 4) due to increase in convection. The perturbation in velocity and temperature due to dissipation is small which is evident from figures 5 and 6. The effect of increase in σ is tc decrease the velocity and temperature distributions because of the dampening effect of the Darcy resistance.

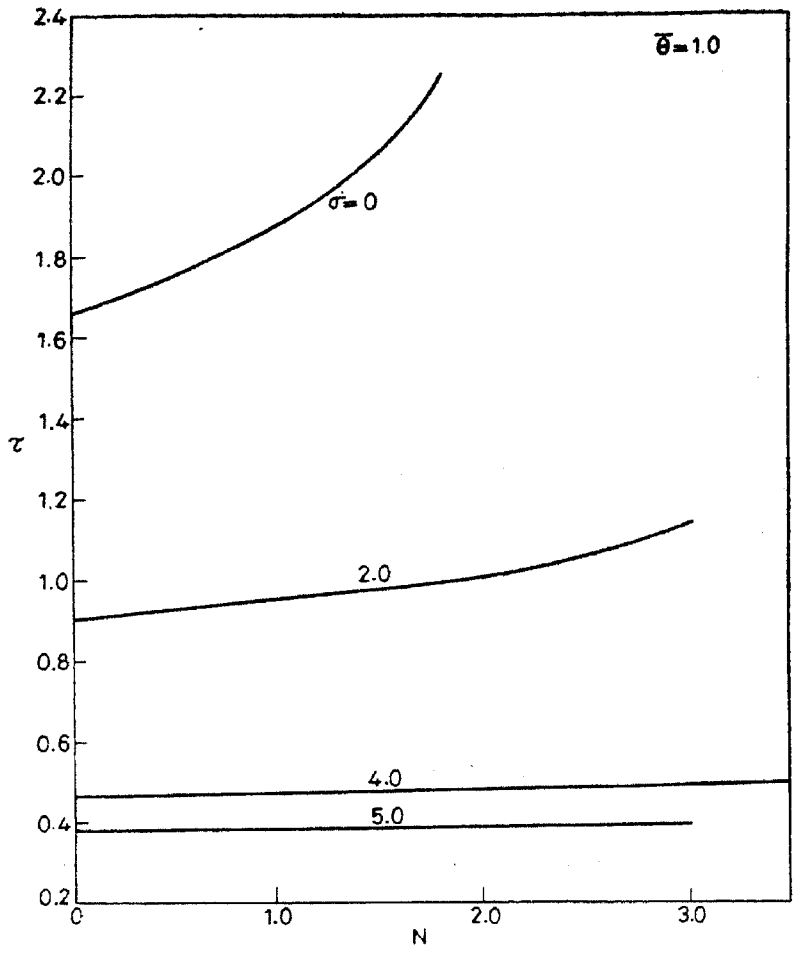

Figure 18. Skin friction *vs.* N at hotter plate.

The ratio of mass flow rate and friction factor with and without porous media, in the absence of dissipative effects, are shown in figures 7 and 8. We see that as σ increases the mass flow rate decreases and friction factor increases. This decrease in mass flow rate with increase in σ is very useful in studying the pore size distribution in a porous medium. The increase in friction factor with increase in σ ensures the laminar flow. The skin friction and rate of heat transfer are computed in the absence of disspative effects for different values of σ and $\bar{\theta}$ and the results are shown in figures 9 to 12. The skin friction increases with increase in $\bar{\theta}$ and decreases with increasing σ. The rate of heat transfer decreases numerically near the hotter plate and increases near the cooler plate with an increase in σ which is evident from the physical grounds explained earlier.

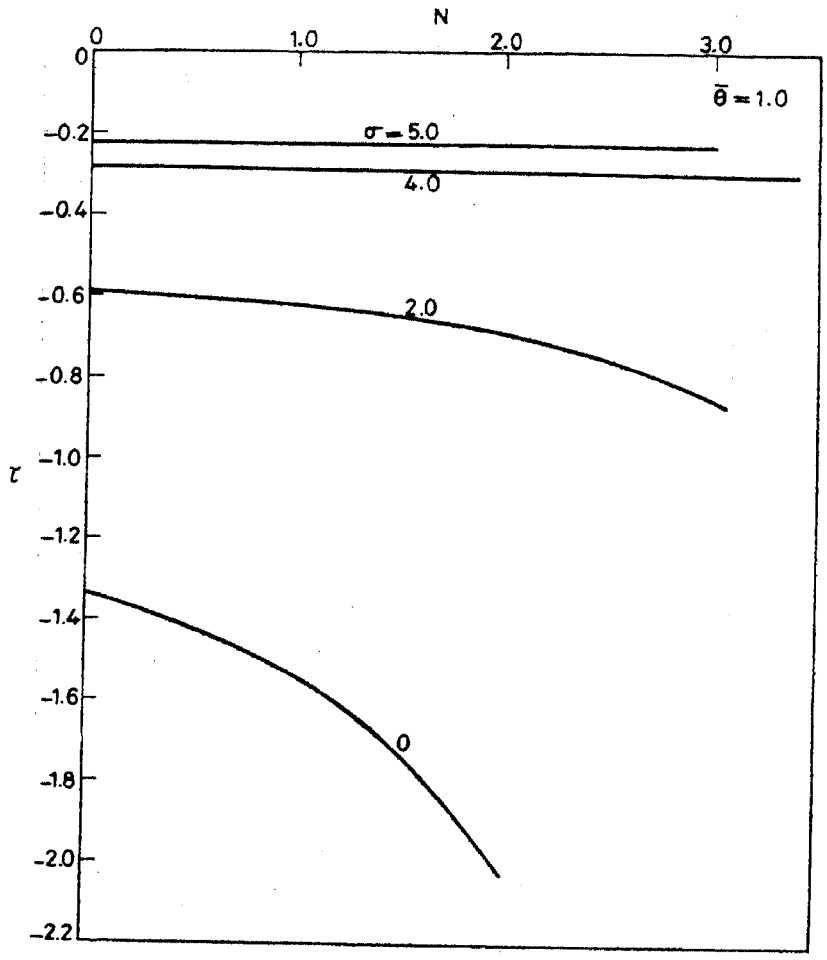

Figure 19. Skin friction *vs.* N at cooler plate.

The above results obtained by the pert urbation method are true only for small values of $N(<1)$. To know up to what values of N the perturbation solutions are valid and to find the effect of large N on the flow, we have solved (8) and (9) numerically using Runge-Kutta-Gill method. The velocity and temperature distributions are obtained for a wide range of values of N and the results are compared with the perturbation solutions in figures 13 and 14. We find that the analytical solutions are in good agreement with the numerical results up to $N=1$ and they deviate considerably for $N>1$. We also observe that the velocity and temperature distribution, increase with increase in N with higher values near the hotter plate than those at the cooler one.

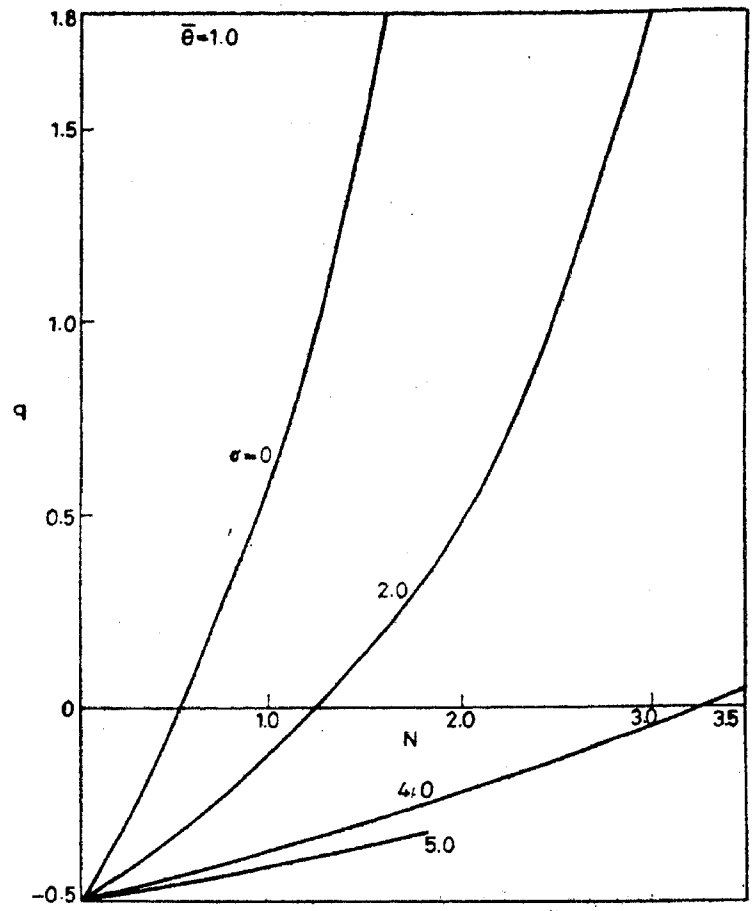

Figure 20. Rate of heat transfer *vs.* N at hotter plate.

The mass flow rate and friction factor in the presence of dissipative effects are computed using the numerical method and the results are shown in figures 15 to 17. From figure 15 it is clear that the increase in N increases the mass flow rate. Although M_p and M_f increase individually with N, their ratio M_p/M_f decreases with N as shown in figure 16. This means that the rate of increase in M_f is much higher than that of M_p. The ratio of friction factor increases with increase in N as shown in figure 17. The skin friction and rate of heat transfer are also computed using the numerical method and the results are shown in figures 18 to 22. We observe that for small values of σ the skin friction increases with N and is independent of N for large values of σ. This is because for small values of σ there exists Taylor-porous boundary layer near the surface in which the velocity gradient is fairly large. For large values of σ the boundary layer type of flow governed by Brinkman model transforms to potential nature of Darcy flow (see Rudraiah and Masuoka [4]) where the velocity gradients are negligibly small. The rate of heat transfer, as shown in figures 20 and 21, increases numerically with N. This is because as N increases the temperature difference also increases resulting in large convection which transfers more heat.

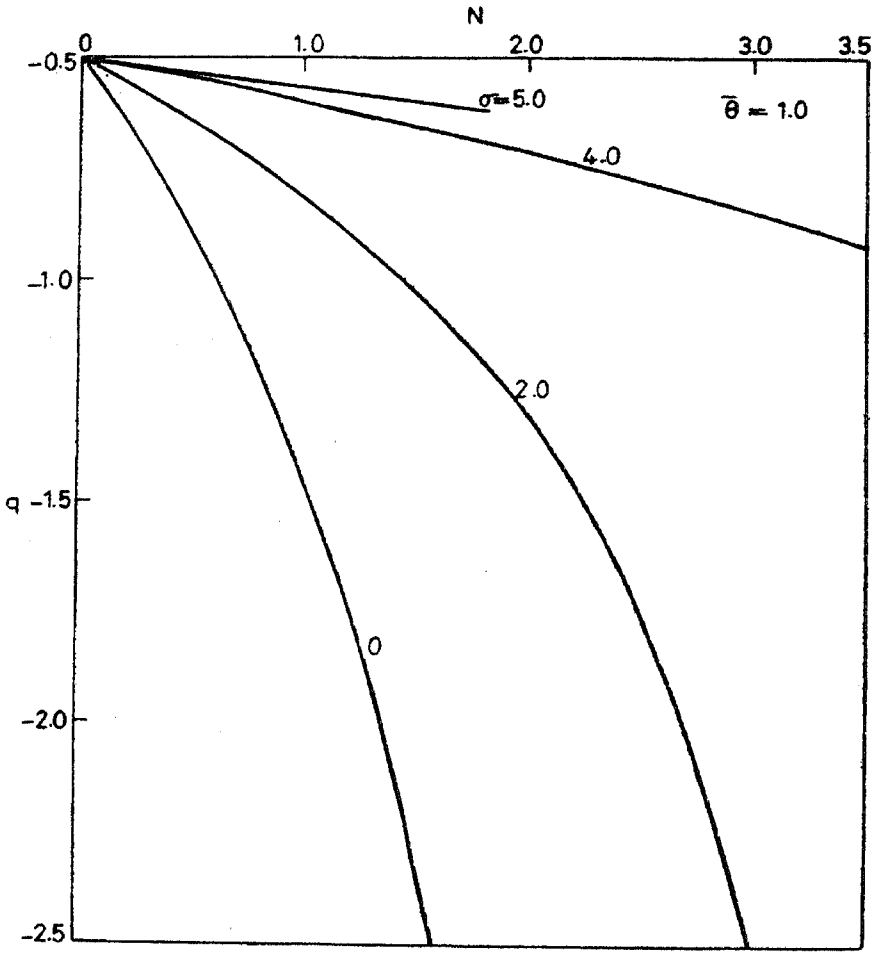

Figure 21. Rate of heat transfer *vs.* N at cooler plate.

Acknowledgements

This work was supported by the UGC India under the DSA scheme. The work of one of the authors (MSM) is supported by the UGC India under its faculty improvement programme. MSM is also grateful to HKE Society for deputing him for higher studies.

References

[1] Brinkman H C 1947 *Appl. Sci. Res.* **A1** 27
[2] Darcy H 1956 Les Fontaines publiques de la Ville de Dijon (Paris : Victor Dalmint)
[3] Gebhart B 1979 *ASME J. Fluid Eng.* **101** 5
[4] Rudraiah N and Masuoka T 1982 *Int. J. Eng. Sci.* **20** 27
[5] Rudraiah N and Nagaraj S T 1977 *Int. J. Eng. Sci.* **15** 589
[6] Sen S K and Venkataramudu V 1976 Report No. CC/SKS-VV/R-04-76 Indian Institute of Science, Bangalore
[7] Wooding R A 1960 *J. Fluid Mech.* **7** 501